The Astrophysical Journal, in preparation
Preprint typeset using LATEX style emulateapj v. 6/22/04

THE IMPACT OF GALAXY FORMATION ON THE SUNYAEV-ZELDOVICH EFFECT OF GALAXY CLUSTERS

Daisuke Nagai
Department of Astronomy and Astrophysics,
Kavli Institute for Cosmological Physics,
5640 S. Ellis Ave., The University of Chicago, Chicago IL 60637
e-mail: daisuke@oddjob.uchicago.edu
The Astrophysical Journal, in preparation

ABSTRACT

We study the effects of radiative cooling and galaxy formation on the Sunyaev-Zel'dovich (SZ) observable-mass relations using high-resolution cosmological simulations. The simulations of eleven individual clusters spanning a decade in mass are performed with the shock-capturing eulerian adaptive mesh refinement N-body+gasdynamics ART code. To assess the impact of galaxy formation, we compare two sets of simulations performed in the adiabatic regime (without dissipation) and with radiative cooling and several physical processes critical to various aspects of galaxy formation: star formation, metal enrichment and stellar feedback. We show that the SZ signal integrated to sufficiently large fraction of the cluster volume correlates strongly with the enclosed cluster mass, regardless of the details of the cluster physics or dynamical state of the cluster. The slope and redshift evolution of the SZ flux-mass relation are also insensitive to the details of the cluster gas physics, and they are well characterized by the simple self-similar cluster model. While the tightness, slope and redshift evolution are relatively unaffected, we show that the radiative cooling and galaxy formation significantly modify the normalization of the SZ scaling relations. In our simulations, we find that the gas cooling and associated star formation suppress the normalization by $\approx 30-40\%$. The effect is due to the decrease in the hot gas fraction, which is offset slightly by the increase in the gas temperature. The baryon dissipation also slightly modifies the cluster mass and affects the normalization by non-negligible amount. Finally, we show that the simulations that include gas cooling and star formation are in good agreement with the recent observational results on the SZ scaling relations obtained using 36 OVRO/BIMA SZ+Chandra X-ray cluster observations, while the simulations neglecting galaxy formation are inconsistent with the observed correlation. The comparison highlights the importance of galaxy formation in theoretical modelling of clusters and shows that the current generation of simulations produce clusters with gross properties quite similar to their observed counterparts.

Subject headings: cosmology: theory–clusters: formation– methods: numerical

1. INTRODUCTION

The Sunyaev-Zel'dovich (SZ) effect is a unique and powerful observational tool for cosmology. It is a small distortion of the cosmic microwave background (CMB) spectrum caused by scattering of CMB photons off a distribution of high energy electrons in dense structures such as clusters of galaxies (Sunyaev & Zeldovich 1970, 1972). This effect has a unique property that the signal is independent of redshift, making it particularly well suited for deep cluster surveys. Such surveys will be able to detect all clusters above a mass limit nearly independently of the redshift of the clusters (e.g., Holder et al. 2000; Weller et al. 2002). The next generation SZ instruments, such as the South Pole Telescope (SPT), should be capable of mapping a fairly large portion of the sky and finding $\gtrsim 10^4$ clusters with masses greater than $\approx 2\times10^{14}M_\odot$ expected to be present out to $z \approx 2$.

A large homogeneous sample of galaxy clusters extending to high redshift will enable direct measurement of the evolution of the number density of galaxy clusters as a function of redshift and provide one of the most powerful constraints on the nature of dark energy (Wang & Steinhardt 1998; Haiman et al. 2001). Indeed, the statistical power of the expected survey yields will be sufficient to constrain the equation of state of dark energy with 5% accuracy (see the review by Carlstrom et al. 2002). However, in order to realize the full statistical power of the upcoming SZ surveys, the systematics would have to be controlled to the comparable level. One of the main sources of the systematic uncertainties lies in the relation between the SZ observable and mass of clusters as a function of redshift. Making this connection is important because the mass of the cluster is not a direct observable. Instead, the clusters would have to be counted as a function of some observable proxy for mass. Therefore, the requirement is to control the systematics in the SZ observable-mass relation to better than about 5% at all redshift (e.g., Carlstrom et al. 2002).

This poses a serious challenge to both observational and theoretical communities. To date, observational studies of SZ scaling relations have been performed using two largest datasets of SZ measurements obtained by the OVRO/BIMA cm-wave imaging experiment (Cooray 1999; McCarthy et al. 2003; LaRoque 2005) and multiband SuZIE experiment (Benson et al. 2004) along with the X-ray observations. Recently, LaRoque (2005) analyzed the sample of 36 clusters observed with both OVRO/BIMA SZ and Chandra X-ray observations. This study showed that a tight correlation exists between the observed SZ flux and X-ray properties of clusters, such as X-ray temperature and derived total and gas masses of clusters. While the observed regularity of the SZ clusters is encouraging, further progress is clearly needed in order to accurately calibrate the relation for the cosmological application. The observational situation is expected to improve rapidly with the advent of a number of dedicated SZ survey instruments, which will dramatically increase the sample size and the number of low-mass clusters.

On the theoretical side, a number of groups have studied the SZ scaling relations using semi-analytic models (Verde et al. 2002; McCarthy et al. 2003) and cosmological cluster simulations (Metzler 1998; White et al. 2002; da Silva et al. 2004; Diaferio et al. 2005; Motl et al. 2005). Motivated by the results of X-ray cluster observations in the past decade (see Voit 2005, for the review and references therein), many of the recent studies have focused on studying the impact of non-gravitational physical processes, such as gas cooling, star formation and energy feedback, on the SZ scaling relations. One of the main results is that the SZ signal integrated to sufficiently large fraction of the cluster volume correlates very strongly with the enclosed cluster mass, independent of the details of the cluster physics or dynamical state of the cluster (see e.g., Motl et al. 2005). The slope and the redshift evolution of the SZ scaling relation also appear to be insensitive to the cluster gas physics (e.g., da Silva et al. 2004). While these results are encouraging for the cosmological applications, the impact of galaxy formation on the normalization is not well understood. As we show below, the normalization is sensitive to the details of cluster gas physics. Because the previous studies used the large number of clusters extracted from large box cosmological simulations, the resolution was inevitably limited to resolve the relevant physics. It is therefore important to check the results of the previous studies and push the theoretical modelling of SZ scaling relations using the high-resolution cluster simulations.

In this paper, we present such study using high-resolution simulations of eleven clusters designed to resolve the formation of cluster galaxies. Although the statistics is limited, these clusters span over a decade in mass and provide good leverage on the scaling relations. The mass resolution of our simulations is more than an order of magnitude higher than that in the previous studies. This work is therefore complimentary to the previous studies in the literature. Using these simulations, we study the impact of gas cooling and galaxy formation on the SZ scaling relations, including the normalization, slope and their redshift evolution. To test the predictions of the numerical simulation, we compare our results to the recent observational results on the SZ scaling relations obtained using the sample of 36 clusters obtained using the OVRO+BIMA SZ and Chandra X–ray telescopes (LaRoque 2005).

The paper is organized as follows. In § 2 we define the observational quantities and present the relevant scaling laws predicted by the self-similar model. We describe the details of our simulations presented in this paper in § 3. In § 4 we present our main results and comparisons to the previous studies and the recent observational results. Finally, in § 5 we discuss our conclusions and their implications the upcoming SZ cluster surveys.

2. THEORETICAL FRAMEWORK

2.1. *Definitions of physical quantities*

The thermal SZ effect is a distortion in the CMB spectrum produced by the inverse Compton scattering of CMB photons off free electrons in dense structures such as clusters of galaxies. The change in the CMB specific intensity caused by the thermal SZ effect at a frequency ν is given by $\Delta I_\nu/I_{\rm CMB} = f_\nu(x)g_\nu(x)y$, for a given line of sight. The dimensionless comptonization parameter y is defined as,

$$y \equiv \frac{k_B\sigma_T}{m_e c^2}\int n_e(l)T_e(l)dl. \tag{1}$$

where n_e and T_e are the number density and temperature of the electrons, m_e is the electron rest mass, c is the speed of light, and σ_T is the Thomson cross-section. There are three frequency dependent factors, including $I_{\rm CMB} = 2h\nu^3/c^2(e^x-1)^{-1}$, $f_\nu(x) = x^4e^x/(e^x-1)^2$ and $g_\nu(x) = x(e^x+1)/(e^x-1)-4$ with $x = h\nu/k_BT_{\rm CMB}$. The corresponding change in the CMB temperature is given by $\Delta T/T_{\rm CMB} = g_\nu(x)y$. In the Rayleigh-Jeans limit ($\nu \ll 200$GHz), $\Delta T/T_{\rm CMB} = -2y$ and $\Delta I_\nu = 2k_B\Delta T\nu^2/c^2$.

Let us now consider the SZ signal arising from a cluster located at redshift z. The SZ flux integrated over the solid angle of observation $d\Omega$ is given by $\Delta S_\nu = \int \Delta I_\nu d\Omega = I_{\rm CMB}f_\nu Y$, where Y is the integrated Compton-y parameter defined as

$$Y \equiv \int_\Omega y d\Omega = \frac{1}{d_A^2(z)}\left(\frac{k_B\sigma_T}{m_ec^2}\right)\int_V n_eT_e dV, \tag{2}$$

$d\Omega = dA/d_A^2(z)$ is the solid angle subtended on the sky, $d_A(z)$ is the angular diameter distance to the cluster at redshift z, and dA and dV are the area and volume of the cluster projected on the sky, respectively. Because Y depends on distance, we will usually work with the intrinsic thermal SZ signal, defined as

$$Y^{\rm int} \equiv Y d_A^2(z) \propto f_{\rm gas}MT_m \tag{3}$$

Note that the integrated SZ flux is linearly sensitive to the gas mass $M_{\rm gas} = f_{gas}M$ and mass-weighted temperature T_m of the cluster, where f_{gas} is the gas fraction and M is the total mass.

2.2. *Self-similar scaling relations*

In the absence of cooling and heating processes, clusters are expected to scale self-similarly to a good approximation (Kaiser 1986). The self-similar model predicts that the temperature of the gas scales with the cluster mass as

$$M \propto T^{3/2}E^{-1}(z) \tag{4}$$

where $M \equiv 4\pi r_\Delta^3\Delta_c\rho_{crit}/3$ is the halo mass enclosed within r_Δ, defined as the radius of a spherical volume within which the mean density is Δ_c times the *critical density*, $\rho_{\rm crit}$, at that redshift (Bryan & Norman 1998). The bracket in Eq. 4 indicates the redshift evolution factor, where $E(z)$ is defined in the redshift-dependent Hubble parameter $H(z) = 100hE(z)$ km s^{-1}Mpc^{-1} with $E^2(z) = \Omega_M(1+z)^3 + \Omega_\Lambda$ in the flat cosmology.

Inserting Eq. 4 into Eq. 3, we obtain the SZ scaling relation predicted by the self-similar model,

$$Y^{\rm int} \propto \begin{cases} f_{\rm gas}M^{5/3}E^{2/3}(z) \\ f_{\rm gas}T^{5/2}E^{-1}(z) \end{cases}. \tag{5}$$

3. SIMULATIONS

In this study, we analyze high-resolution cosmological simulations of eleven cluster-size systems in the "concordance" flat ΛCDM model: $\Omega_{\rm m} = 1 - \Omega_\Lambda = 0.3$, $\Omega_{\rm b} = 0.04286$, $h = 0.7$ and $\sigma_8 = 0.9$, where the Hubble constant is defined as $100h$ km s^{-1} Mpc^{-1}, and σ_8 is the power spectrum normalization on $8h^{-1}$ Mpc scale. The simulations were done with the Adaptive Refinement Tree (ART) N-body+gasdynamics code (Kravtsov 1999; Kravtsov et al. 2002), a Eulerian code that uses adaptive refinement in space and time, and (non-adaptive) refinement in mass (Klypin et al. 2001) to reach the high dynamic range required to resolve cores of halos formed in self-consistent cosmological simulations.

To set up initial conditions we first ran a low resolution simulation of $80h^{-1}$ Mpc and $120h^{-1}$ Mpc boxes and selected eleven clusters with the masses ranging from $M_{500c} \approx 3.5 \times 10^{13}$ to $9 \times 10^{14} h^{-1}$ M$_\odot$. The properties of clusters at the present epoch are listed in Table 1. The perturbation modes in the lagrangian region corresponding to the sphere of several virial radii around each cluster at z=0 was then re-sampled at the initial redshift, $z_i = 25$ for the three most massive clusters (CL1-3) and $z_i = 49$ for the remaining eight clusters in the sample. For the three most massive clusters we have resampled radius of $3R_{\rm vir}(z{=}0)$, while for the rest of the clusters the resampling sphere had radius of $5R_{\rm vir}(z{=}0)$, where $R_{\rm vir}(z{=}0)$ is the virial radius enclosing overdensities of $\Delta_{\rm vir} = 334$ with respect to the mean density of the universe at z=0. During the resampling we retained the previous large-scale waves intact but included additional small-scale waves, as described by Klypin et al. (2001). The resampled lagrangian region of each cluster was then re-simulated with high dynamic range.

High-resolution simulations were run using 128^3 uniform grid and 8 levels of mesh refinement in the computational boxes of $120h^{-1}$ Mpc for CL1-CL3 and $80h^{-1}$ Mpc for CL4-CL11, which corresponds to the dynamic range of $128 \times 2^8 = 32768$ and peak formal resolution of $80/32,768 \approx 2.44h^{-1}$ kpc, corresponding to the actual resolution of $\approx 2 \times 2.44 \approx 5h^{-1}$ kpc. Only the region of $\sim 3 - 10h^{-1}$ Mpc around the cluster was adaptively refined, the rest of the volume was followed on the uniform 128^3 grid. The mass resolution corresponds to the effective 512^3 particles in the entire box, or the Nyquist wavelength of $\lambda_{\rm Ny} = 0.469h^{-1}$ and $0.312h^{-1}$ *comoving* megaparsec for CL1-3 and CL4-11, respectively, or $0.018h^{-1}$ and $0.006h^{-1}$ Mpc in the physical units at the initial redshift of the simulations. The dark matter particle mass in the region around the cluster was $9.1 \times 10^8 h^{-1}$ M$_\odot$ for CL1-3 and $2.7 \times 10^8 h^{-1}$ M$_\odot$ for CL4-CL11, while other regions were simulated with lower mass resolution.

As the zeroth-level fixed grid consisted of only 128^3 cells, we started the simulation already pre-refined to the 2nd level ($l = 0, 1, 2$) in the high-resolution lagrangian regions of clusters. This is done to ensure that the cell size is equal to the mean interparticle separation and all fluctuations present in the initial conditions are evolved properly. During the simulation, the refinements were allowed to the maximum $l = 8$ level and refinement criteria were based on the local mass of DM and gas in each cell. The logic is to keep the mass per cell approximately constant so that the refinements are introduced to follow the collapse of matter in a quasi-lagrangian fashion. For the DM, we refine the cell if it contains more than two dark matter particles of the highest mass resolution specie. For gas, we allow the mesh refinement, if the cell contains gas mass larger than four times the DM particle mass scaled by the baryon fraction. In other words, the mesh is refined if the cell contains the DM mass larger than $2(1 - f_b)m_p$ or the gas mass larger than $= 4f_b m_p$ (where m_p is given above and $f_b = \Omega_{\rm b}/\Omega_{\rm m} = 0.1429$). We analyze clusters at the present-day epoch as well as their progenitors at higher redshifts.

We repeated each cluster simulation with and without radiative cooling. The first set of "adiabatic" simulations have included only the standard gasdynamics for the baryonic component without dissipation and star formation. The second set of simulations included gasdynamics and several physical processes critical to various aspects of galaxy formation: star formation, metal enrichment and thermal feedback due to the supernovae type II and type Ia, self-consistent advection of metals, metallicity dependent radiative cooling and UV heating due to cosmological ionizing background (Haardt & Madau 1996). We will use labels 'ad' and 'csf' for the adiabatic simulations and simulations with cooling and star formation, respectively.

The cooling and heating rates take into account Compton heating and cooling of plasma, UV heating, atomic and molecular cooling and are tabulated for the temperature range $10^2 < T < 10^9$ K and a grid of metallicities, and UV intensities using the `Cloudy` code (ver. 96b4, Ferland et al. 1998). The Cloudy cooling and heating rates take into account metallicity of the gas, which is calculated self-consistently in the simulation, so that the local cooling rates depend on the local metallicity of the gas. Star formation in these simulations was done using the observationally-motivated recipe (e.g., Kennicutt 1998): $\dot{\rho}_* = \rho_{\rm gas}^{1.5}/t_*$, with $t_* = 4 \times 10^9$ yrs. The code also accounts for the stellar feedback on the surrounding gas, including injection of energy and heavy elements (metals) via stellar winds and supernovae and secular mass loss. The detailed description and implementation of the star formation and stellar feedback are provided in Kravtsov et al. (2005).

The high-resolution and the inclusion of various physical processes critical to galaxy formation enable unique studies of the impact of galaxy formation on the properties of the ICM. The mass resolution of the simulation is sufficiently high to resolve the galactic-size halos as small as $1/10,000$ of the mass of the host cluster (Nagai & Kravtsov 2005), and the observed properties of the cluster galaxies are well reproduced in the current simulations (Nagai et al. 2005b, in preparation). These simulations have been used to study the effects of galaxy formation on the gas fractions in clusters (Kravtsov et al. 2005). The main results of this paper is that gas cooling and star formation significantly suppress the gas fraction within the virial radius of the cluster. The comparisons of the simulations to the recent deep Chandra X-ray observations of nearby clusters further showed that the current simulations reproduce the observed gas fractions remarkably well (Kravtsov et al. in preparation). Because the SZ signal is proportional to the cluster gas fraction, these results indicate that the impact of galaxy formation on

TABLE 1
Simulated cluster sample of the CSF run at z=0

Name	R_{500c}	M_{500c}^{gas}	M_{500c}^{tot}	$\langle T_{\rm spec}\rangle$
	h^{-1}Mpc	$h^{-1}10^{13}M_\odot$	$h^{-1}10^{14}M_\odot$	keV
CL1	1.160	8.19	9.08	10.0
CL2	0.976	5.17	5.39	8.1
CL3	0.711	1.92	2.09	4.1
CL4	0.609	1.06	1.31	2.7
CL5	0.661	1.38	1.68	3.9
CL6	0.624	1.22	1.41	3.2
CL7	0.522	0.74	0.82	1.7
CL8	0.487	0.43	0.67	2.2
CL9	0.537	0.78	0.90	2.2
CL10	0.509	0.62	0.77	2.1
CL11	0.391	0.27	0.35	1.2

the SZ flux may also be significant.

Throughout this paper we use estimates of $Y^{\rm int}$, mass and other cluster observables within different commonly used radii, defined by the total matter overdensity they enclose. We will use radii r_{2500}, r_{500}, r_{200} enclosing overdensities of $\Delta_c = 2500$, 500, and 200 with respect to the critical density, $\rho_{\rm crit}$, as well as radii r_{180} and $r_{\rm vir}$ enclosing overdensities of $\Delta_m = 180$ and $\Delta_{\rm vir}$ with respect to the mean density of the universe. The latter is equal to $\Delta_{\rm vir} \approx 334$ at z=0 and ≈ 200 at z=1 for the cosmology adopted in our simulations. The virial radius and masses of clusters within r_{500c} for the CSF run at z=0 are given in Table 1. For reference, we also give the spectral X-ray temperature, $\langle T_{\rm spec}\rangle$, of individual clusters extracted from the mock Chandra analysis (Nagai et al. 2005, in preparation). The spectral temperature, $\langle T_{\rm spec}\rangle$, is equivalent to the single-temperature fit to the total cluster spectrum in the radial range 70 kpc $< r < r_{500c}$.

4. RESULTS

In this section, we study the impact of gas cooling and galaxy formation on the SZ scaling relations using the cosmological cluster simulations. Our general strategy is to assess the effects of various physical processes on the cluster observables and the scaling relations by comparing the simulations with and without radiative cooling and star formation.

4.1. *Pressure Profiles*

Since the SZ effect is sensitive to the pressure of the ICM, we will start with the analysis of the pressure profiles. Figure 1 shows the comparisons of the mean pressure profiles at z=0 and z=1 for our entire sample of clusters simulated in the adiabatic regime and with gas cooling and star formation. To compute the mean profiles, we first normalize the differential and cumulative pressure profiles of individual clusters using the mean integrated pressure within the sphere of r_{500c}, denoted as $\bar{P}_{500c}$, and plot them as a function of the cluster-centric radius in units of r_{500c}. The mean profiles are computed by averaging the normalized profiles over the entire cluster sample. To highlight the impact of gas cooling and star formation on the pressure profiles, we normalize the profiles of the CSF run using $\bar{P}_{500c}$ of the adiabatic run for each cluster. The shaded bands show the 1σ rms scatter around the mean profile of the CSF run. The mean and scatter of the profiles are computed for the logarithm of pressure.

The Figure shows that the simulated clusters ranging in an order of magnitude in mass show remarkably similar pressure profiles at all radii. The differential pressure profile declines by nearly four orders of magnitude from the center to r_{500c}, and the scatter is small ($\approx$ 20%) throughout the cluster. In the outskirts of the cluster, the rate of decline is generally faster than that of the gas density profile and the gravitationally dominant dark matter. This is because the pressure is the product of the gas density and temperature for the ideal gas, and the latter also declines with radius (see Motl et al. 2005; Vikhlinin et al. 2005b). For example, the typical power-law slope of the differential pressure profile is ≈ -3.5 at r_{500c}, which is steeper than the typical slope of the density profile of ≈ -3 seen in the cosmological simulations (Navarro et al. 1996, 1997) as well as the recent X-ray observations (Vikhlinin et al. 2005a).

One of the main results from this analysis is that the pressure is suppressed throughout the cluster in the CSF runs compared to the adiabatic runs. The cumulative pressure at r_{500c}, for example, is suppressed by $\approx$ 25% on average, and this effect is relatively constant ($\approx$ 25−35%) in the region outside $> 0.2r_{500c}$ at z=0. In the cluster center, the pressure is significantly more concentrated, and its profile becomes steeper, because the potential is deeper and the density profile is steeper due to the baryon dissipation and the contraction of dark matter (Gnedin et al. 2004). Note, however, that this high pressured cluster core contributes very little to the cumulative pressure at large radii. For example, the inner regions within $< 0.1r_{500c}$ contributes less than 2% of the total SZ signal within r_{500c}. Thus, the SZ signal integrated out to a sufficiently large radius is insensitive to the gas properties in the cluster core.

Although the general trends are similar, the suppression of pressure varies more strongly with radius at z=1, because a dense, cool core dominates the larger fraction of r_{500c} at high redshift. Nevertheless, we find that the suppression of the cumulative pressure at r_{500c} is comparable at z=0 and 1. However, the difference becomes more apparent in the inner regions; for example, the effect at r_{2500c} changes from 35% at z=0 to 20% at z=1. If a similar trend exists in real clusters this implies that the redshift evolution of the SZ scaling relation is expected to deviate from the prediction of the self-similar model, if the SZ observable is computed within the aperture considerably smaller than r_{500c}.

In order to better understand the suppression of the pressure profile, it is useful to study the impact of gas cooling and star formation on the gas density, temperature and entropy profiles. The Figure 2 shows that the suppression of the pressure is accompanied by the strong suppression in the gas density and the moderate increase in the gas temperature. The entropy profile provides further insights into these phenomena, because it uniquely characterizes the pressure, gas density and temperature

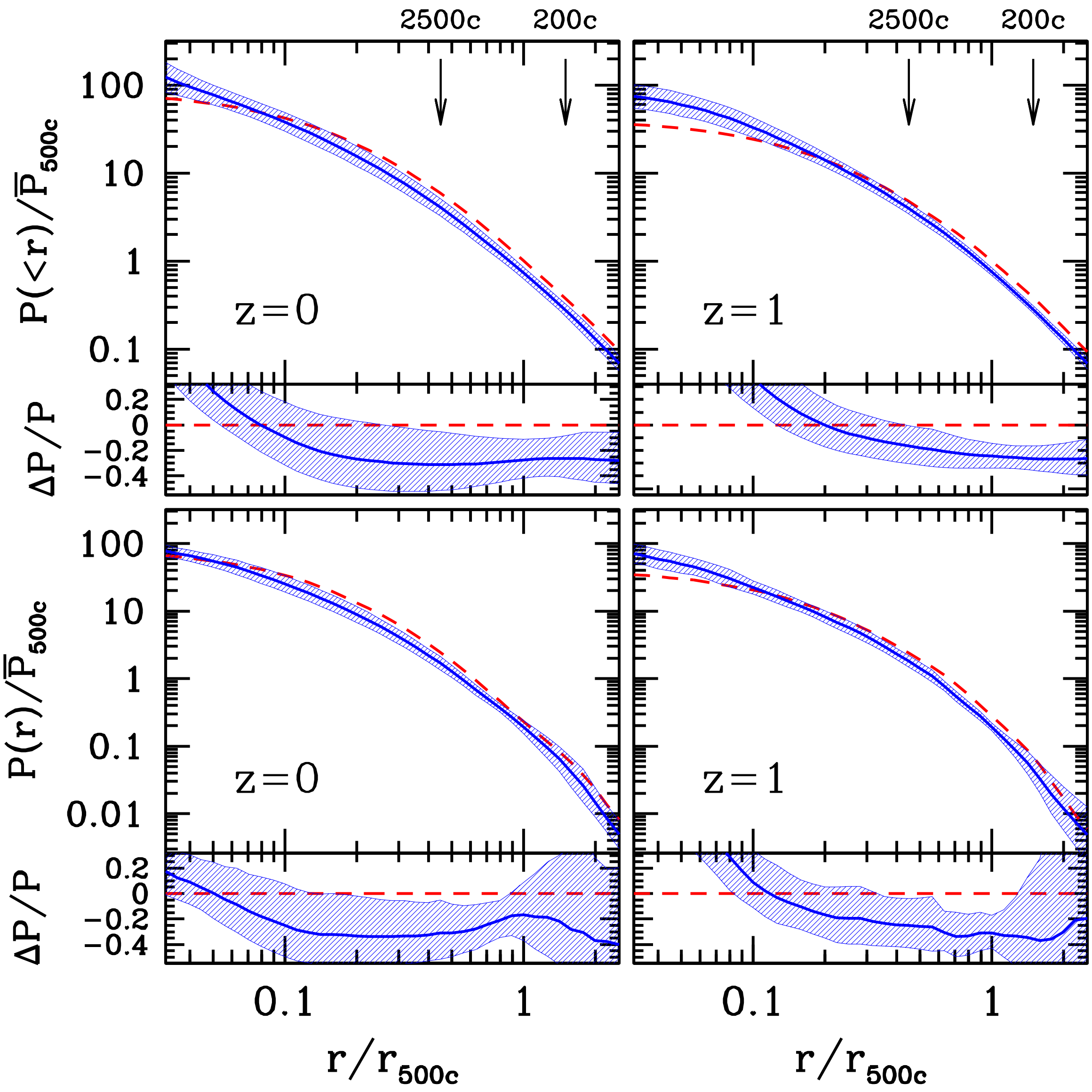

FIG. 1.— Cumulative (*top panels*) and differential (*bottom panels*) pressure profiles for the eleven clusters used in our analysis at z=0 (*left column*) and z=1 (*right column*). The *dashed* lines show the mean profiles in the adiabatic simulations averaged over eleven clusters. The *solid* lines show the mean profiles in the simulations with cooling and star formation. Note that all profiles are normalized to the mean cumulative pressure at r_{500c} in the adiabatic runs, $\bar{P}_{500c}$, at each epoch. The *bottom panel* of each figure shows the fractional deviation of the mean profile of the CSF run relative to the mean profile of the adiabatic run. In all panels, the shaded bands show the 1σ *rms* scatter around the mean for the eleven clusters. The vertical arrows in the top panels show the radii enclosing overdensities of 2500 and 200 with respect to the critical density at each epoch.

profiles of the ICM, given the shape of its confining potential well (see Voit et al. 2002 and references therein). The Figure 2 shows that the entropy of gas, defined as $S \equiv T/n^{2/3}$, is enhanced throughout the cluster out to $2 \times r_{500c}$. The effect peaks around $0.3r_{500c}$, and the entropy is enhanced by about 40% at r_{500c}. In our simulations, gas cooling and star formation can increase the entropy of gas in one of two ways: (1) the high entropy gas from outside flows in to replenish the gas removed by gas cooling in the inner region (**?**) or (2) the direct heating of the ICM by the energy injection from supernova explosions. The former is likely a dominant mechanism that shapes the overall entropy distribution, while the second process is important for regulating the rate of gas cooling in the high density region (e.g., the vicinity of the central galaxy and the cluster galaxies), where stars are forming with sufficiently high rate.

To examine the mass dependence of the effects, we split the sample in half and show the mean profiles of the six most massive and five least massive clusters in the Figure 2. The Figure shows that the shape and the normalization of the pressure profiles show the smallest systematic trend with mass. In the outskirt of the clusters $> 0.3r_{500c}$, we find similarly small systematic trend with mass for the gas density, temperature and entropy profiles. In the inner region, on the other hand, we find slightly more pronounced mass dependence in

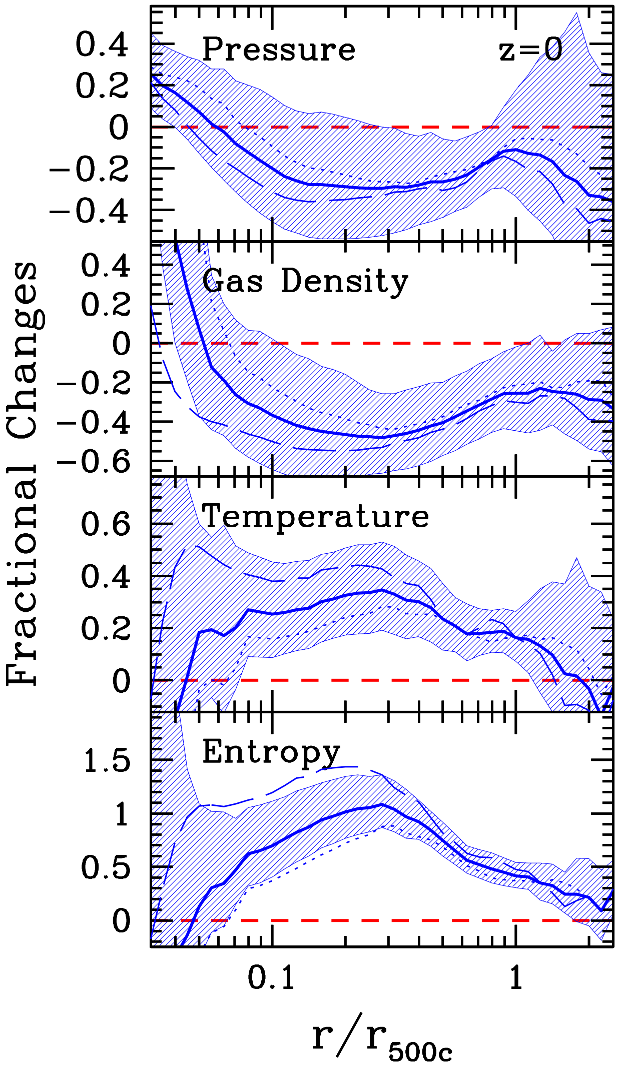

FIG. 2.— Impact of gas cooling and star formation on the pressure, gas density, temperature and entropy profiles (*from top to bottom*) of the simulated clusters at z=0. The *solid* lines show the fractional changes of the mean differential radial profiles in the CSF simulations averaged over eleven clusters relative to the mean profiles in the adiabatic runs, indicated by the line at zero. The *dotted* and *dashed* lines show the same for the subsamples of six most and five least massive clusters in our sample, respectively. Note that the mean profile of each quantity is computed by first normalizing the profiles of each cluster by the value of the cumulative profile at r_{500c} and averaging these normalized profiles over the samples.

all profiles. Among them, the pressure profile shows the smallest trend with mass. In less massive clusters, we find that the changes in gas density and temperature become larger. Since the signs of these changes are opposite, these effects cancel each other to give the smallest mass dependence on pressure. In contrast, the effects add constructively to give the largest mass dependence of entropy.

The main conclusion from this analysis is that the cooling and star formation suppress the amplitude of the gas pressure and therefore the SZ signal, and the effect depends rather weakly on the mass of the cluster. These results imply that the processes of galaxy formation will modify the normalization of the SZ observable-mass relation, but its impact on the slope of the relation is expected to be small. This is the main topic of the discussion in the next section.

4.2. *The SZ scaling relations*

We will start with the SZ flux-total mass (SZ-M) relation because this is the relation directly relevant for the cosmological application. Figure 3 shows the comparison of the SZ-total mass scaling relation at r_{500c} and its redshift evolution for the sample of eleven clusters in the adiabatic and CSF runs. At each epoch, we performed the fits to the entire sample of simulated clusters using a simple power-law relation,

$$Y = A_{14} \times 10^{-6} \left(\frac{M}{10^{14} h^{-1} M_{\odot}} \right)^{\alpha_M}, \qquad (6)$$

where A_{14} is the normalization at $10^{14}h^{-1}M_{\odot}$ in units of 10^{-6} and α_M is the slope. In practice, we fit a straight line to the log(Y)-log(M) relation by minimizing the χ^2. The values of the best-fit normalization and slope measured at different radii, including r_{180m}, $r_{\rm vir}$, r_{200c}, r_{500c} and r_{2500c}, are listed in Table 2. The values in the adiabatic simulations are marked 'ad', while those in the simulations with cooling and star formation are marked 'csf' (e.g., $A_{14}^{\rm csf}$). The best-fit parameters in the Table and the right panel of the Figure 3 are obtained by fitting the normalization and slope simultaneously. To highlight any deviation from the self-similar slope, the best-fit relations shown in the left panel of the Figure 3 are obtained by fixing the slope to 5/3. Note that fixing the slope to 5/3 for the fits changes the best-fit normalization by no more than 5% at both z=0 and z=1.

In the right panel of the Figure 3, the errorbars indicate 2σ confidence region of the best-fit slope and normalization in the CSF simulations at each epoch. Since the redshift evolution of the normalization is measured relative to the relation at z=0, the errorbars at $z>0$ include the uncertainties in the best-fit normalizations at each epoch and z=0 added in quadrature. Note also that the sizes of the errorbars are comparable for the adiabatic simulations. The errorbars shown in the Figures 5 and 6 are also computed in the same way.

The left panel shows that the SZ signal integrated within the sphere of r_{500c} correlates very strongly with the enclosed cluster mass at both z=0 and 1. The rms scatter is about 10-15% in both adiabatic and cooling runs. Moreover, we find that the slope of the adiabatic run is in very good agreement with the predicted slope of the self-similar model. The best-fit slope of the CSF run is also not very different from the predicted slope of 5/3, but there is an indication that the slope may be systematically steeper by $\lesssim 0.1$. Unfortunately, however, the current sample size is too small to rule out the predicted slope of the self-similar model with statistical significance. A larger sample of simulated clusters is clearly needed to assess this effect in the future studies.

While the tightness and the slope of the relations are relatively unaffected, gas cooling and star formation significantly modify the normalization of the SZ-total mass relation. Compared to the adiabatic run, the normalization of the CSF run is lower by 41, 34 and 27% at r_{2500c}, r_{500c} and r_{180m}.

The right panel shows that the redshift evolution of the SZ-total mass relation is consistent with the prediction

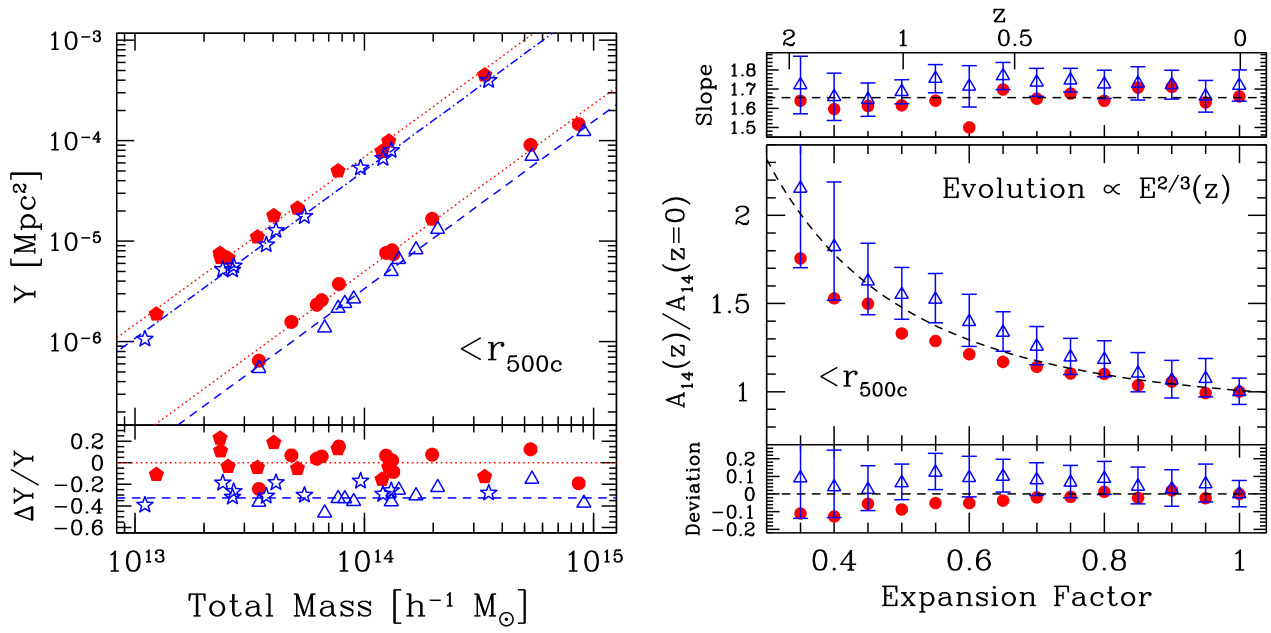

FIG. 3.— The SZ flux-total mass relations for the eleven clusters in the adiabatic (*solid symbols*) and cooling (*open symbols*) simulations. *Left-top panel:* the relation between the integrated compton-Y vs. total mass enclosed within the sphere of radius r_{500c} at z=0 (*bottom lines and points*) and z=1 (*top lines and points*). The *solid circles* and *solid pentagons* are the adiabatic runs at z=0 and 1, while the *open triangles* and *open stars* are the cooling runs at these epochs, respectively. At each epoch, the *dotted* and *dashed* lines show the best-fit relations for the adiabatic and cooling runs with the slope fixed at the self-similar value of 5/3. For clarity, the z=1 relations are shifted upward by a factor of ten. *Left-bottom panel:* the fractional deviation of individual clusters from the best-fit relation of the adiabatic runs at each epoch. The *dashed* line indicates the best-fit relation of the cooling runs at z=0. *Right panel:* the redshift evolution of the slope (*top*) and the normalization (*middle*) of the SZ flux-total mass relation between z=2 and the present day. The *solid circles* and *open triangles* indicate the adiabatic and cooling runs, respectively. The *dashed* lines indicate the slope of 5/3 (*top*) and the evolution of normalization predicted by the self-similar model (*middle*). The errorbars indicate 2σ confidence region of the best-fit slope and normalization in the CSF runs at each epoch. The *bottom* panel shows the fractional deviation of the best-fit normalization from the self-similar prediction as a function of time.

of the self-similar model in the entire redshift range considered here. First, the slope is constant with redshift. Second, the redshift evolution of the normalization is in good agreement with the predicted evolution of the self-similar model. We also find similar results at other radii considered in this paper.

To better understand the impact of galaxy formation on the SZ scaling relation, we also examine their effects on f_{gas} and T_m in the Figure 4. Compared to the adiabatic run, we find that f_{gas} is lower by 38% in the CSF run; however, its effect on the SZ observable is offset partially by the increase in T_m by 9%. The net effect is the reduction of the SZ signal by 29%, which falls short of the 34% change in the normalization of the SZ-M relation. This illustrates that the changes in f_{gas} and T_m alone do not fully account for the change in the normalization.

In addition, we find that the baryon dissipation slightly modifies the total mass of the cluster (see also Kravtsov et al. 2005, in preparation). Our simulations show that the median increase in M_{tot} at r_{500c} is about 7%. The effect becomes larger at the smaller radii, and the effect is about 20% at r_{2500c}. This effect will cause the shift in the SZ-M relation in both x- and y-directions by the same amount. However, since the slope of the relation is $\approx$5/3, the 7% shift in the positive x-axis translates into the 12% shift in the negative y-axis. The net effect is therefore the negative 5% change in the normalization due to the change in M_{tot}. Putting them all together, we find that the 34% decrease in the normalization of the SZ-M relation at r_{500c} is due to the combined effects of 38% decrease in f_{gas}, 9% increase in T_m and the net 5% decrease due to the change in M_{tot}. Note also that the inclusion of gas cooling and star formation causes decrease in the SZ signal and M_g within r_{500c} by 22% and 31%, respectively.

Finally, we check the redshift evolution of f_{gas} and T_m. The self-similar model predicts that f_{gas} is constant with time, while T_m of a given mass evolves with time according to the Eq. 4. To examine the deviation from the predicted evolution, the Figure 5 plots the deviation of the best-fit normalization of the $f_{gas} - M$ and $T_m - M$ relations at $M_{500c} = 10^{14}h^{-1}M_\odot$ from the predicted evolution as a function of redshift. The Figure shows that f_{gas} and T_m of a given mass in the CSF runs deviate from the predicted evolution of the self-similar model, while the evolution in the adiabatic runs is consistent with the self-similar model. In the CSF runs, the deviation increases toward higher redshifts. On average, f_{gas} is higher by about 12% at z=1 and 17% at z=2 compared to its value at z=0, while T_m is lower by an almost equal amount at each epoch. Since the SZ signal is linearly proportional to both of these quantities, the evolution in f_{gas} is canceled almost exactly by the evolution in T_m. Note also that we did not find systematic

TABLE 2
THE NORMALIZATION AND SLOPE OF THE SZ SCALING RELATIONS AT z=0

	SZ-Total Mass				SZ-Gas Mass				SZ-Temperature			
Δ	$A_{14}^{\rm ad}$	$\alpha_M^{\rm ad}$	$A_{14}^{\rm csf}$	$\alpha_M^{\rm csf}$	$A_{13}^{\rm ad}$	$\alpha_{M_g}^{\rm ad}$	$A_{13}^{\rm csf}$	$\alpha_{M_g}^{\rm csf}$	$A_5^{\rm ad}$	$\alpha_T^{\rm ad}$	$A_5^{\rm csf}$	$\alpha_T^{\rm csf}$
180m	2.59	1.63	1.88	1.68	1.55	1.63	2.19	1.60	18.24	2.52	12.06	2.60
vir	3.11	1.61	2.20	1.67	1.86	1.61	2.61	1.60	14.11	2.52	9.18	2.63
200c	3.78	1.62	2.56	1.70	2.29	1.62	3.24	1.60	9.98	2.50	6.37	2.62
500c	4.99	1.66	3.29	1.73	3.08	1.65	4.59	1.60	5.97	2.45	3.63	2.61
2500c	8.82	1.68	5.22	1.77	6.31	1.64	9.27	1.58	2.10	2.50	1.19	2.73

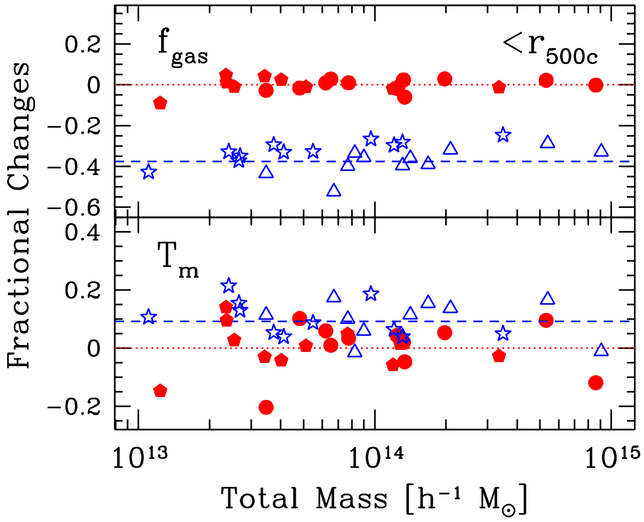

FIG. 4.— Fractional changes in the gas mass fraction (*top*) and mass-weighted temperature (*bottom*) enclosed within the sphere of radius r_{500c} between the adiabatic and CSF simulations as a function of cluster mass. The *solid circles* and *solid pentagons* are the adiabatic runs at z=0 and 1, while the *open triangles* and *open stars* are the cooling runs at these epochs, respectively. The fractional deviation of the gas mass fractions in the individual clusters from the mean gas mass fraction of the adiabatic runs at each epoch, indicated by the *dotted line* at zero. The *dashed* line indicates the best-fit relation of the cooling runs at z=0.

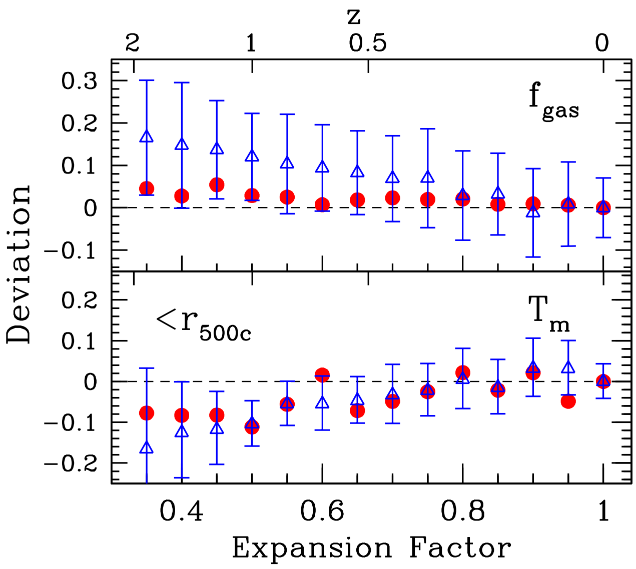

FIG. 5.— The evolution of the gas mass fraction (*top*) and mass-weighted temperature (*bottom*) at $M_{500c} = 10^{14}h^{-1}M_\odot$. The fractional deviation of the best-fit normalization from the self-similar prediction, indicated by the *dashed* line. The errorbars indicate 2σ statistical uncertainties in the CSF runs at each epoch.

evolution in the impact of the baryon dissipation on the total mass with redshift. This explains why the SZ signal of a given mass shows very little evolution beyond the evolution predicted by the self-similar model.

So far, we have focused on the SZ-total mass relation because of its direct relevance for the cosmological studies. Unfortunately, however, the cluster mass is not a direct observable, and making the unbiased observational measurements of the SZ-M relation is difficult. Therefore, it is also useful to study the relations between the SZ signal and the global properties of cluster that can be measured more reliably from the observations. This can provide a useful direct test of the simulations.

Here, we consider two such quantities, including the gas mass, M_g, and mass-weighted temperature, T_m, of the cluster. Figure 6 shows the SZ-M_g and SZ-T_m relations at r_{500c} and the redshift evolution of their slope and normalization. At each timestep, we perform the fits to the entire sample of simulated clusters using the following simple power-law relations,

$$Y = A_{13} \times 10^{-6}\left(\frac{M_g}{10^{13}h^{-1}M_\odot}\right)^{\alpha_{M_g}} \quad (7)$$

$$Y = A_5 \times 10^{-5}\left(\frac{T_m}{5\mathrm{keV}}\right)^{\alpha_T} \quad (8)$$

where A_{13} is the normalization at $10^{13}h^{-1}M_\odot$ in units of 10^{-6} and α_{M_g} is the slope of the SZ-M_g relation. Similarly, A_5 is the normalization at 5 keV in units of 10^{-5} and α_T is the slope of the SZ-T_m relation. The Table 2 lists the values of the best-fit normalization and slope

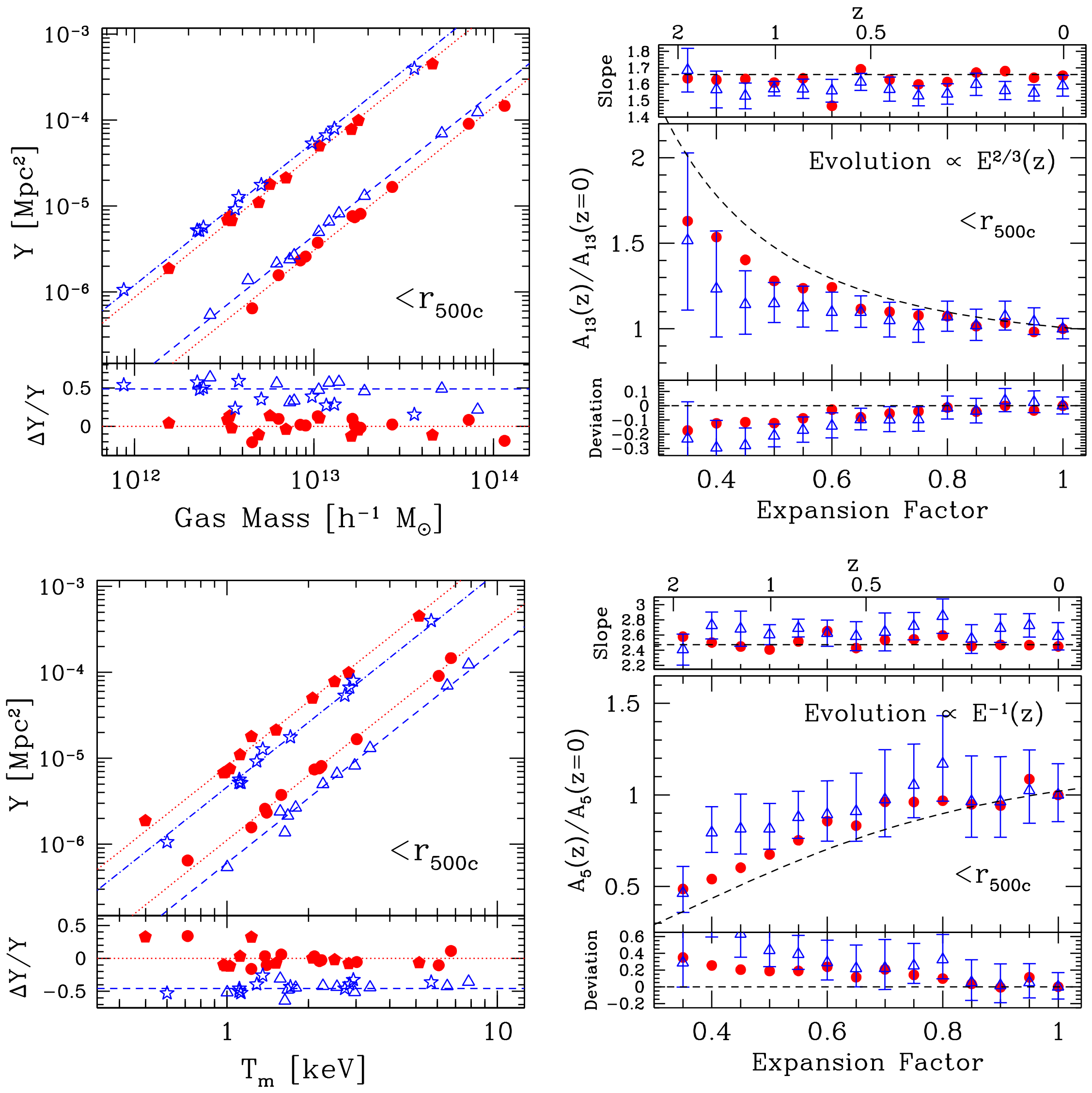

FIG. 6.— *Top panels:* the SZ flux-gas mass relations. The *left panel* shows the scaling relations at z=0 (*bottom lines and points*) and 1 (*top lines and points*). The *right panel* shows the redshift evolution of the slope and normalization between z=2 and 0. The errorbars indicate 2σ confidence region of the best-fit slope and normalization in the CSF runs at each epoch. Point and line types are the same as in Fig. 3. *Bottom panels:* the relation between the SZ flux and the mass weighted temperature.

measured at different radii for the z=0 sample. The errorbars shown in the Figure indicate 2σ confidence region of the best-fit slope and normalization in the CSF runs at each epoch.

The Figure shows that both SZ-M_g and SZ-T_m relations are as equally tight as the SZ-M relation. The best-fit slopes of the adiabatic runs are in very good agreement with the predicted slope of the self-similar model. The best-fit slopes of the CSF runs, on the other hand, are marginally consistent with the predicted slope, and there are indications that the slopes in the CSF run may be slightly smaller (larger) for the SZ-M_g(SZ-T_m) relations. We also find that the slope is constant with time in both the adiabatic and CSF runs.

While the tightness and the slopes of these relations are relatively unaffected, gas cooling and star formation have a large impact on their normalization. Figure 6 shows that the normalization of the CSF run is higher by 49% in the SZ-M_g relation at r_{500c}, while it is lower by 39% in the SZ-T_m relation at the same radius. Note that the change in the normalization of the SZ-M_g relation has opposite sign from the change in the SZ-M relation, because gas cooling and star formation significantly reduce the gas mass of the cluster. Recall that the inclusion of gas cooling and star formation reduces the SZ signal by 22% and M_g by 31% at r_{500c}. For the slope of 5/3, the decrease in M_g by 31% in the x-direction corresponds to the increase of the normalization by 52%. The net effect is therefore the increase of the normalization by 30% at r_{500c}. Similar accounting works for the SZ-T_m relation as well. We also find that the impact of galaxy formation on the normalization becomes larger in the inner region of the cluster.

In contrast to the SZ-M relation, we find that the inclusion of gas cooling and star formation modifies the redshift evolution of the normalization in the SZ-M_g and

SZ-T_m relations. In the CSF run, we find that the normalization of the SZ-M_g relation is systematically lower by ≈20% at z=1 than the predicted normalization of the self-similar evolution model, while the SZ-T_m relation is higher by ≈40% at z=1. The departure from the predicted evolution is mainly due to the evolution in f_{gas} and T_m, not the SZ signal, as discussed above (see also the Figure 5). Note also that the redshift evolution of the adiabatic simulations is consistent with the self-similar model at all redshift within the errors.

4.3. *Comparisons to Previous Work*

We now compare the results of our simulations to the previous studies in the literature (White et al. 2002; da Silva et al. 2004; Motl et al. 2005). So far, all of the previous studies have used a large number of clusters extracted from large box cosmological simulations. While these simulations provide good statistics, the resolution is inevitably limited to resolve the relevant physical processes. The present work is on the other end of the spectrum: the resolution is high, but the statistics is low. In this sense, our work is complimentary to the previous studies. Thus, the comparisons of the different types of work will provide useful insights at the both ends of the spectrum.

Using the SPH simulations, da Silva et al. (2004) studied the SZ scaling relations in adiabatic simulations and re-simulations in which gas was allowed to cool or was pre-heated. These studies showed that both strong gas cooling and preheating modify the slope of the SZ-M relation. They find that the slope in the cooling run ($\alpha_M = 1.79$) was steeper than the slope of the adiabatic run ($\alpha_M = 1.69$) by about 0.1. More recently, Motl et al. (2005) used the large sample of clusters simulated using a eulerian AMR code and studied the SZ-M relation in the adiabatic run and three resimulations in which they added gas cooling, star formation and feedback one at a time. These studies showed that the slope in the simulations that include both cooling and star formation is very similar to the slope in the adiabatic run. Similar results are obtained using the simulations performed with the entropy conserving Gadget code with cooling, star formation and feedback (White et al. 2002). The results of our simulations are also consistent with these findings. Moreover, Motl et al. (2005) showed that the slope in the cooling only run is steeper than the slope in the adiabatic run by 0.1, consistent with the results reported by da Silva et al. (2004).

In addition to the scatter and slope of the relation, da Silva et al. (2004) investigated their redshift evolution. They showed that the slope and normalization of the SZ-M relation evolve with redshift according to the the self-similar model out to z=2 in their adiabatic and cooling only run. Motl et al. (2005) also found similar results in all four sets of their simulations up to z=1.5. We reached the same conclusions using the high-resolution simulations.

In summary, the scatter, slope and redshift evolution of the SZ observable-mass relation are generally insensitive to the details of the cluster gas physics. These results appear to be very robust. In fact, the agreement among different studies is rather remarkable, because these studies used the simulations carried out using very different numerical techniques, resolution and implementation of

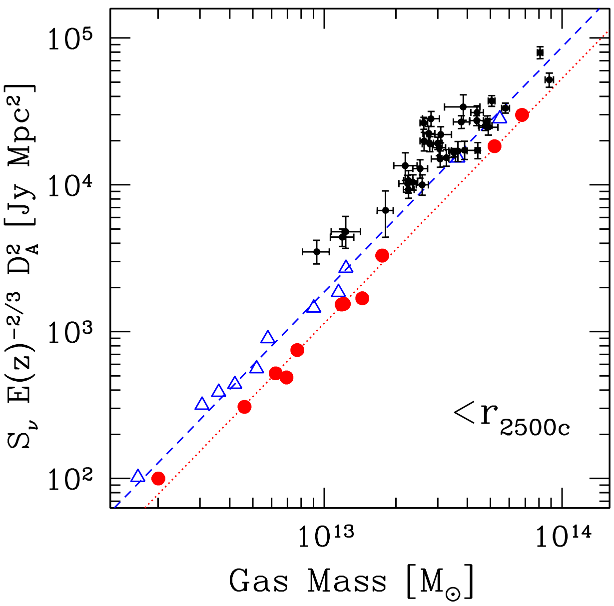

FIG. 7.— Comparisons of the SZ flux-gas mass relations in the simulations and observations. The *data points with errorbars* show the BIMA/OVRO SZ+Chandra X–ray cluster observations for a sample of 36 clusters (LaRoque 2005). The SZ flux is the integrated flux within the 2D projected aperture of R_{2500c}, while the gas mass is the enclosed gas mass within the sphere of r_{2500c}. The SZ flux is also corrected for the redshift evolution assuming the self-similar evolution model and the ΛCDM cosmology. The *solid circles* and *open triangles* show the eleven simulated clusters in the adiabatic and cooling and star formation runs, respectively, at z=0. The *dotted* and *dashed* lines are the best-fit relations at z=0 of each set of simulation. The figure shows that the simulations that include gas cooling and star formation are in reasonably good agreement with the data, while the adiabatic simulations are inconsistent with the observed relation.

various physical processes incorporated in the simulations.

Despite the robustness of the results discussed so far, the impact of galaxy formation on the normalization of the SZ observable-mass relation is not yet well understood, because the magnitude of the effect is closely related to the cold baryon fractions, which have not yet converged among different simulations. da Silva et al. (2004), for example, find that the normalization of the SZ-M relation in their cooling only run is lower by 20% and 9% at $M_{200c} = 10^{14}$ and $5\times10^{14}h^{-1}M_\odot$ compared to the adiabatic run, respectively. Moreover, White et al. (2002) discusses even smaller impact of galaxy formation in their simulation, because of the efficient energy feedback model used to regulate conversion of the hot gas into stars (Springel & Hernquist 2002). Using our high-resolution simulations, we report that gas cooling and associated star formation cause the decrease in the normalization of the SZ-M relation by 41, 34 and 32% at r_{2500c}, r_{500c} and r_{200c}, respectively, almost uniformly throughout the cluster mass range. This is one of the largest impacts on the SZ scaling relation reported to date.

4.4. *Comparisons to Observations*

To gauge how well the current simulations compare to the data, we compare the scaling relations in our simulations to the recent observational results. Figure 7 shows the comparisons of the SZ flux-gas mass relation from our simulations to the recent observational results based on the sample of 36 clusters observed with SZ BIMA/OVRO interferometers and Chandra X-ray telescope (LaRoque 2005). The cluster sample includes clusters in a broad redshift range from z=0.14 to z=0.89. For the comparison, we use the SZ observable-gas mass relation, rather than the SZ-total mass relation, because the gas mass can be measured more accurately using the Chandra X-ray cluster observations (see LaRoque 2005, for details). The SZ flux is the integrated flux within the 2D projected aperture of R_{2500c}, while the gas mass is the enclosed gas mass within the sphere of r_{2500c}. These quantities are computed from the best-fit isothermal β model, fit jointly to the SZ and Chandra data (see LaRoque 2005, for details). The observed SZ flux at a given redshift is also corrected for the redshift evolution assuming the canonical self-similar model and the ΛCDM cosmology.

In the simulations, the SZ flux is computed by projecting the sphere of $3 \times r_{500c}$ centered around the minimum of the cluster potential. Note that the hot gas in the outskirts of the cluster makes non-negligible contribution to the SZ signal, if the projected aperture is a small fraction of the virial radius of the cluster. For the projected radius of R_{2500c}, we find that 35% of the SZ signal arises from the region outside the sphere of r_{2500c}, on average. Although we find no systematic variation of the projection effect with the mass of the cluster, we find significant variation of the effect among different clusters at a level of about 20%. The contribution of the cluster outskirts becomes less significant as we make the projected aperture larger. The projection of the hot gas associated with the dense structures in the foreground or background of the cluster is not accounted for in this comparison.

The comparison shows that the simulations that include gas cooling and star formation are in reasonable agreement with the data, while the adiabatic simulations are inconsistent with the observed relation. This comparison therefore highlights the importance of galaxy formation in theoretical modelling of clusters and shows that the current generation of simulations produce clusters with gross properties very similar to their observed counterparts.

5. DISCUSSION & CONCLUSIONS

We have presented the analysis of the Sunyaev-Zel'dovich (SZ) scaling relations using the high-resolution simulations of galaxy clusters formed in the concordance ΛCDM cosmology. The simulations of eleven individual clusters spanning a decade in mass ($M_{500c} = 3.5 \times 10^{13}$ to $9 \times 10^{14} h^{-1} M_{\odot}$) are performed with the shock-capturing eulerian adaptive mesh refinement N-body+gasdynamics ART code. We study the effects of gas cooling and star formation on the SZ scaling relations and their redshift evolution between z=0 and z=2 by comparing two sets of simulations performed with and without these processes included. The main results are summarized as follows.

1. The SZ signal integrated to sufficiently large fraction of the cluster volume correlates very strongly with the enclosed total cluster mass, independent of the details of the cluster physics or dynamical state of the cluster. The rms scatter of the SZ-total mass relation is about 10-15%.
2. The slope of the relation in the adiabatic run is in very good agreement with the predicted slope of the self-similar model in the entire probed redshift range. We find that the impact of the galaxy formation on the slope is small ($\lesssim 0.1$).
3. The redshift evolution of the SZ-total mass relation is consistent with the self-similar model between z=0 and z=2: (a) the slope is constant with redshift and (b) the normalization evolves with redshift according to the self-similar evolution model.
4. Gas cooling and star formation significantly modify the normalization of the SZ observable-total mass relation. The inclusion of these physical processes causes the decrease in the normalization of the relation by 41, 34 and 27% at r_{2500c}, r_{500c} and r_{180m}, respectively. The decrease is due to the large decrease in the gas fraction, which is offset somewhat by the increase in the mass weighted temperature. The baryon dissipation also modifies the total mass of the cluster and hence affects the normalization by about 5%.
5. The integrated SZ signal also correlates strongly with the gas mass and temperature of the clusters. The results (1)-(3) apply equally well for these scaling relations, except that the redshift evolution of the normalization exhibits deviation from the self-similar model increasing toward higher redshift. Gas cooling and star formation also significantly modify the normalization of these relations.
6. The SZ observable-gas mass relation in the simulations that include gas cooling and star formation is in reasonably good agreement with the observed relation recently obtained using the sample of 36 OVRO/BIMA SZ+Chandra X-ray observations (LaRoque 2005), while the simulations neglecting galaxy formation are inconsistent with the observed correlation.

These results have a number of important implications for the cosmological studies with the upcoming SZ cluster surveys. First and foremost, the SZ fluxes of clusters exhibit remarkable regularity at all redshifts, and the SZ signal integrated to sufficiently large fraction of the cluster volume is insensitive to the merging events (see e.g., Motl et al. 2005) or the properties of the cluster core (see § 4.1). This indicates that the integrated SZ flux is extremely good proxy for the total cluster mass. Second, we showed that the slope and redshift evolution of the relation are insensitive to the details of cluster gas physics, and they are well characterized by the simple self-similar cluster model between z=0 and 2. The simplicity of the redshift evolution of the slope and normalization implies that the self-calibration (Hu 2003; Majumdar & Mohr 2004) will be effective. Finally, these results appear to be very robust. In § 4.3, we showed that the same conclusions have been reached using the simulations with very different numerical techniques, resolution and implementation of various physical processes incorporated in the simulations.

Despite the simplicity of the redshift evolution, the normalization of the SZ flux-mass relation is much less well understood, because the magnitude of the effect is closely related to the cold baryon fraction, which has not yet converged among different simulations. Using the high-resolution cluster simulations, we show that the radiative cooling and galaxy formation have significant impact on the normalization of the SZ scaling relations. In our simulations, we find that the inclusion of gas cooling and star formation suppress the normalization by $\approx 30-40\%$, primarily due to the large reduction in the gas fractions. Interestingly, the SZ scaling relations in the simulations are in reasonably good agreement with the recent observational results. The gas fractions in the simulations also compare well with the measurements from deep Chandra X–ray observations of nearby clusters (Kravtsov et al. in preparation). Despite these successes in matching the SZ and X–ray observations, the current cluster simulations may still suffer from the "overcooling" problem: the fraction of baryons in the cold gas and stars within the virial radius of clusters at z=0 in our simulations is in the range 0.25-0.35, at least a factor of two higher than observational measurements (see Kravtsov et al. 2005, and references therein). The problem appears to be in the central brightest cluster galaxy, which contains a larger fraction of cluster stellar mass than is measured in observations. At the same time, the discrepancy may also be partly in the observed stellar fraction; for example, some fraction of cluster stellar mass in low-surface brightness intracluster component are missed in observations (e.g., Gonzalez et al. 2005; Lin & Mohr 2004).

Given the importance of these issues, further efforts from observers and theorists are needed to understand the SZ scaling relations to the level required for the cosmological studies. Observationally, it is important to increase the sample size and the number of low-mass clusters. Comparisons of different instruments will also help resolve systematic differences among different instruments (see e.g., Benson et al. 2005). It is also critical to understand the systematics in the measurements of the cluster mass through detailed and extensive comparisons of X–ray, SZ and lensing cluster observations. With the advent of a number of dedicated SZ survey instruments, the observational situation is expected to improve rapidly.

Theoretically, it is important to push the detailed theoretical modelling using the high-resolution cluster simulations to investigate the role of various processes, such as thermal conduction and AGN feedback, in suppressing cooling and star formation in cluster cores and their impact on the global properties of the cluster. For the cosmological application, it is also critical to understand the projection effects (White et al. 2002) and the nature of scatter in the observable-mass relation (Lima & Hu 2005). The high-resolution large box cluster simulations will likely provide important insights into these issues and help assess the effectiveness of the self-calibration technique (Hu 2003; Majumdar & Mohr 2004) in deriving the cosmological constraints from the future SZ cluster surveys.

I would like to thank Andrey Kravtsov and John Carlstrom for their invaluable guidance and advice during the course of this Ph.D. project. I would also like to thank Sam LaRoque for many useful discussions on the SZ observations and providing the data points for the comparisons with the simulations. I also thank Wayne Hu, Clem Pryke and Gus Evrard for useful comments and suggestions on the manuscript. This project was supported by the NASA Graduate Student Researchers Program and by NASA LTSA grant NAG5–7986. The cosmological simulations used in this study were performed on the IBM RS/6000 SP4 system (`copper`) at the National Center for Supercomputing Applications (NCSA).

REFERENCES

Benson, B. A., Church, S. E., Ade, P. A. R., Bock, J. J., Ganga, K. M., Henson, C. N., & Thompson, K. L. 2004, ApJ, 617, 829
Bryan, G. L. & Norman, M. L. 1998, ApJ, 495, 80
Carlstrom, J. E., Holder, G. P., & Reese, E. D. 2002, ARA&A, 40, 643
Cooray, A. R. 1999, MNRAS, 307, 841
da Silva, A. C., Kay, S. T., Liddle, A. R., & Thomas, P. A. 2004, MNRAS, 348, 1401
Diaferio, A., Borgani, S., Moscardini, L., Murante, G., Dolag, K., Springel, V., Tormen, G., Tornatore, L., & Tozzi, P. 2005, MNRAS, 356, 1477
Ferland, G. J., Korista, K. T., Verner, D. A., Ferguson, J. W., Kingdon, J. B., & Verner, E. M. 1998, PASP, 110, 761
Gnedin, O. Y., Kravtsov, A. V., Klypin, A. A., & Nagai, D. 2004, ApJ, 616, 16
Gonzalez, A. H., Zabludoff, A. I., & Zaritsky, D. 2005, ApJ, 618, 195
Haardt, F. & Madau, P. 1996, ApJ, 461, 20
Haiman, Z., Mohr, J. J., & Holder, G. P. 2001, ApJ, 553, 545
Holder, G. P., Mohr, J. J., Carlstrom, J. E., Evrard, A. E., & Leitch, E. M. 2000, ApJ, 544, 629
Hu, W. 2003, Phys. Rev. D, 67, 081304
Kaiser, N. 1986, MNRAS, 222, 323
Kennicutt, R. C. 1998, ApJ, 498, 541
Klypin, A., Kravtsov, A. V., Bullock, J. S., & Primack, J. R. 2001, ApJ, 554, 903
Kravtsov, A. V. 1999, PhD thesis, New Mexico State University
Kravtsov, A. V., Klypin, A., & Hoffman, Y. 2002, ApJ, 571, 563
Kravtsov, A. V., Nagai, D., & Vikhlinin, A. A. 2005, ApJ, 625, 588
LaRoque, S. 2005, PhD thesis, University of Chicago
Lima, M. & Hu, W. 2005, PRD submitted (`astro-ph/0503363`)
Lin, Y.-T. & Mohr, J. J. 2004, ApJ, 617, 879
Majumdar, S. & Mohr, J. J. 2004, ApJ, 613, 41
McCarthy, I. G., Babul, A., Holder, G. P., & Balogh, M. L. 2003, ApJ, 591, 515
Metzler, C. A. 1998, unpublished (`astro-ph/9812295`)
Motl, P. M., Hallman, E. J., Burns, J. O., & Norman, M. L. 2005, ApJ, 623, L63
Nagai, D. & Kravtsov, A. V. 2005, ApJ, 618, 557
Navarro, J. F., Frenk, C. S., & White, S. D. M. 1996, ApJ, 462, 563
—. 1997, ApJ, 490, 493
Springel, V. & Hernquist, L. 2002, MNRAS, 333, 649
Sunyaev, R. A. & Zeldovich, Y. B. 1970, Comments on Astrophysics and Space Physics, 2, 66
—. 1972, Comments on Astrophysics and Space Physics, 4, 173
Verde, L., Haiman, Z., & Spergel, D. N. 2002, ApJ, 581, 5
Vikhlinin, A., Kravtsov, A., Forman, W., Jones, C., Markevitch, M., Murray, S. S., & V., S. L. 2005a, ApJ submitted (astro-ph/0507092)
Vikhlinin, A., Markevitch, M., Murray, S. S., Jones, C., Forman, W., & V., S. L. 2005b, ApJ in press (astro-ph/0412306)
Voit, G. M. 2005, Rev.Mod.Phys., 77, 207
Wang, L. & Steinhardt, P. J. 1998, ApJ, 508, 483
Weller, J., Battye, R. A., & Kneissl, R. 2002, Physical Review Letters, 88, 231301
White, M., Hernquist, L., & Springel, V. 2002, ApJ, 579, 16